Microstructural evolution and mechanical properties of ultrafine grained Al₃Ti/Al–5.5Cu composites produced via hot pressing and subsequent friction stir processing

Q. Zhang [a,b], B.L. Xiao [a], P. Xue [a], Z.Y. Ma [a,*]

[a] *Shenyang National Laboratory for Materials Science, Institute of Metal Research, Chinese Academy of Sciences, 72 Wenhua Road, Shenyang 110016, China*
[b] *University of Science and Technology of China, 96 Jinzhai Road, Hefei 230026, China*

A B S T R A C T

In situ Al₃Ti/Al–5.5Cu composites fabricated by powder metallurgy and subsequent forging were subjected to multiple pass friction stir processing (FSP) with and without active cooling. The forged sample exhibited lower strength and ductility due to the presence of coarse Al₃Ti clusters with a size range of 50–100 μm and coarse matrix grains. Four-pass FSP in air resulted in the refinement and redistribution of the Al₃Ti clusters, and the generation of micron matrix grains, thereby increasing the strength and ductility of the composites. Furthermore, coarse Al₂Cu particles dissolved and re-precipitated due to a relatively long duration of thermal exposure. Additional two pass FSP with rapid water cooling (FSP-water) dissolved most of the Al₂Cu into the matrix and retained the solutes in solution due to the short duration of thermal exposure. Meanwhile, ultrafine matrix grains with a high density of dislocations were obtained. These microstructural changes led to significant increase in strength and a decrease in ductility in the FSP-water sample. After aging, the FSP-water sample exhibited further increased yield strength and ultimate tensile strength due to the precipitation of metastable Al₂Cu phases. However, the ductility did not decrease due to the decrease of dislocation density after aging.

© 2012 Elsevier B.V. All rights reserved.

1. Introduction

Particle reinforced aluminum matrix composites (PRAMCs) are a class of advanced materials providing ideal properties such as high specific strength, high specific modulus and good wear resistance. They have successfully found applications in aerospace and automobile industries [1–3]. Generally, various ceramic particles such as SiC and Al₂O₃ are used as reinforcements due to relatively low density and high elastic modulus [2–5]. However, high thermal mismatch stress due to the large difference of coefficient of thermal expansions (CTE) between the ceramic particles and the Al matrix resulted in poor thermal fatigue resistance when subject to thermal cycles [6]. Al₃Ti particles would be an alternative due to the closer CTE to the Al matrix [7]. Furthermore, Al₃Ti has high specific strength, high specific modulus and excellent mechanical properties at both ambient and elevated temperatures [8].

In previous studies, Al₃Ti/Al composites have been fabricated via stir-casting and powder metallurgy (PM) [9–11]. However, the Al₃Ti particles in the composites were usually greater than 20 μm due to the high process temperature or the coarse raw material powders [9–11]. The coarse Al₃Ti blocks tend to crack under low

stress during tensile testing, resulting in low strength and ductility. Chianeh et al. [9] suggested that decreasing the size of initial Ti powders would shorten the time of complete phase transformation from Ti to Al₃Ti and decrease the size of Al₃Ti, thereby improving the strength of the Al₃Ti/Al composites. However, it is costly to use the fine Ti powder (<5 μm) as a raw material. Therefore, it is highly desirable to develop a method of forming the fine Al₃Ti particles in situ in the Al matrix, or breaking up and distributing homogeneously the Al₃Ti particles.

Friction stir processing (FSP) has developed from a technique called friction stir welding (FSW). It is a new solid state processing technique for microstructural modification [12]. A number of investigations indicate that FSP is an effective technique to refine and redistribute the second phase particles in cast alloys and metal matrix composites, and to fabricate the Al matrix composites reinforced by in situ Al₂Cu, Al₃Ti, and Al₃Fe [13–17]. Furthermore, for precipitation-hardened alloys, FSP causes most of the precipitates to dissolve into the matrix, with re-precipitation occurring during FSP cooling or subsequent aging [18,19]. Additionally, FSP produces fine, equiaxed, recrystallized grains in the stir zone (SZ), with ultrafine grains being obtained in 7075Al and pure Cu plates via FSP with active rapid cooling [20,21].

In a previous study [22], in situ Al₃Ti particles reinforced pure Al composites were fabricated using an Al–Ti system by means of reactive hot pressing and subsequent FSP. It was indicated that FSP

* Corresponding author. Tel.: +86 24 83978908; fax: +86 24 83978908.
E-mail address: zyma@imr.ac.cn (Z.Y. Ma).

Fig. 1. Processing route of the composites.

Fig. 2. XRD pattern of forged in situ Al$_3$Ti/Al–5.5Cu composite.
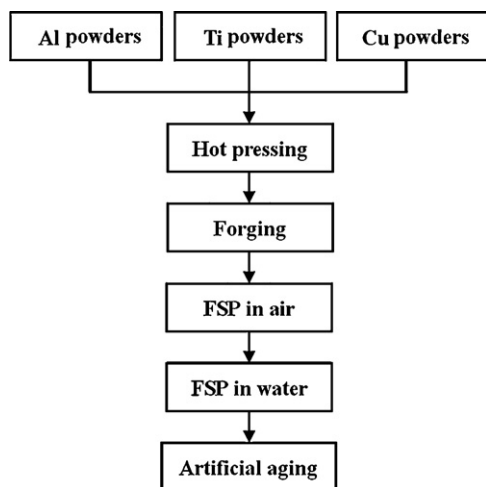
could break-up and homogenize the Al$_3$Ti particles and enhance the reaction between Ti and Al, thereby increasing the mechanical properties of the composites significantly. In order to increase the strength of the composites further, an Al–Ti–Cu system was used in this study to fabricate the in situ Al$_3$Ti/Al–Cu composites by reactive hot pressing and subsequent FSP. Furthermore, active cooling in flowing water was employed for some FSP runs to refine the matrix grain size and prohibit the precipitation of the precipitates during FSP cooling. The aim of the present study is to (a) investigate the effect of Cu addition on the Al–Ti reaction, (b) understand the effect of cooling condition on the grain refinement and the dissolution and precipitation of the precipitates during FSP, and (c) develop an effective approach to enhance the mechanical properties of the in situ composites.

2. Experimental procedure

The starting materials used in this study were Al powder (99.9% purity, 13 μm), Ti powder (99% purity, 45 μm) and Cu powders (99% purity, 75 μm). Assuming all the Ti reacted with Al to form Al$_3$Ti, the volume fraction of Al$_3$Ti would be 23%, and the nominal composition of the matrix would be Al–5.5Cu (wt%). The processing route of the composites in this study is shown in Fig. 1.

The Al, Ti and Cu powders were mixed in a bi-axis rotary mixer for 12 h, and then the mixed powders were hot pressed after being held at 600 °C for 120 min. The hot pressed billets were forged into pancakes at 480 °C with a reduction of 80% in height. The forged plates were subjected to 4-pass FSP with 100% overlapping in air at a rotation rate of 1000 rpm and a traverse speed of 25 mm min^{-1} (defined as FSP-air). Some FSP-air samples were subjected to additional 2-pass FSP, with 100% overlap in flowing water at a rotation rate of 1000 rpm and a traverse speed of 200 mm min^{-1} (defined as FSP-water). The samples were first fixed in room temperature water and additional rapid cooling using flowing water was used during FSP. The thickness of the water layer in the flume was approximately 50 mm. A steel tool with a concave shoulder 20 mm in diameter and a threaded conical pin 8 mm in root diameter, 5.5 mm in tip diameter and 4 mm in length was used for FSP both in air and water. The thermocouples were embedded at the bottom of the SZ to acquire the temperature profiles of the FSP runs. Some FSP-water samples were aged at 175 °C for 4 h.

The samples for microstructural investigations were cut in a direction transverse to the FSP. The microstructures were examined by optical microscopy (OM, Axiovert 200 MAT), scanning electron microscopy (SEM, Quanta 600), complemented by
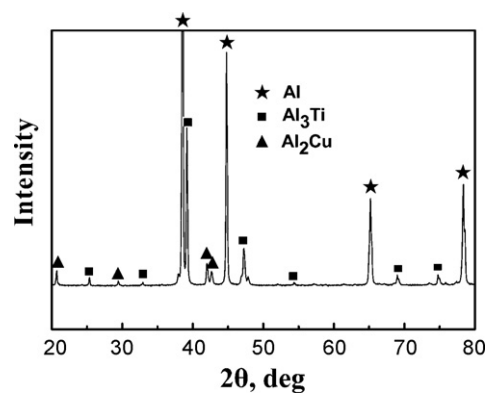
energy-dispersive spectroscopy (EDS), transmission electron microscopy (TEM, TECNAI20), and differential scanning calorimetry (DSC, TA-Q1000). Thin foils for TEM were prepared by the ion-milling technique. The heating rate of DSC was 10 °C min^{-1}. Dogbone-shaped tensile specimens (5.0 mm gauge length, 1.4 mm gauge width and 1.0 mm gauge thickness) were electrical discharge machined from the SZ of the FSP samples transverse to the FSP direction. Density of the forged sample was measured using Archimedean principle. Tensile tests were conducted using an INSTRON 5848 micro-tester at an initial strain rate of 1 × 10^{-3} s^{-1}. The values for each condition were calculated by averaging three test results. After tensile testing, the fracture surfaces were examined using SEM.

3. Results

3.1. Microstructure

Fig. 2 shows the XRD pattern of the forged sample. Peaks of Al$_3$Ti and Al$_2$Cu were revealed, with no peaks corresponding to Ti and Cu detected. This indicates that all the Ti and Cu reacted with the Al to form Al$_3$Ti and Al$_2$Cu. Fig. 3 shows the microstructures of the forged sample. Besides some equiaxed grains, some elongated grains with the size of 10–20 μm were found in the matrix (Fig. 3(a)). Some gray clusters 50–100 μm were observed in the dark Al matrix (Fig. 3(b)). High magnification SEM images revealed that these clusters consisted of numerous particles 1–4 μm in diameter (Fig. 3(c)). Some white particles were usually located in the matrix or the clearance of the clusters. EDS analysis indicated that the gray particles were Al$_3$Ti, and the white particles were Al$_2$Cu (Fig. 3(d) and (e)). Furthermore, no residual porosity was found and the density of the forged sample was measured to be 2.936 g cm^{-3}, which reached the 99.6% of the theoretical density of the composites (2.943 g cm^{-3}). This indicates that the billet almost attained full densification after hot pressing and forging.

Fig. 4 shows the SEM images of the FSP-air and FSP-water samples, respectively. After 4-pass FSP in air, the distribution of Al$_3$Ti becomes homogeneous. The average size of Al$_3$Ti revealed by SEM was approximately 1–3 μm. Some Al$_2$Cu particles were found near the Al$_3$Ti. Additional 2-pass FSP in water caused little influence on the size and distribution of Al$_3$Ti particles. However, the Al$_2$Cu particles disappeared after FSP in water.

Fig. 5 shows the TEM images of the FSP-air sample. The intermetallics located near the Al$_3$Ti particles were identified to be Al$_2$Cu by electron diffraction pattern (Fig. 5(a) and (d)). The grains of the Al matrix, with relatively low density of dislocations, were approximately 1.5 μm (Fig. 5(b)). Some fine Al$_3$Ti particles about 100–200 nm distributed at the grain boundaries and within the grain interiors were also observed. After additional 2-pass FSP in
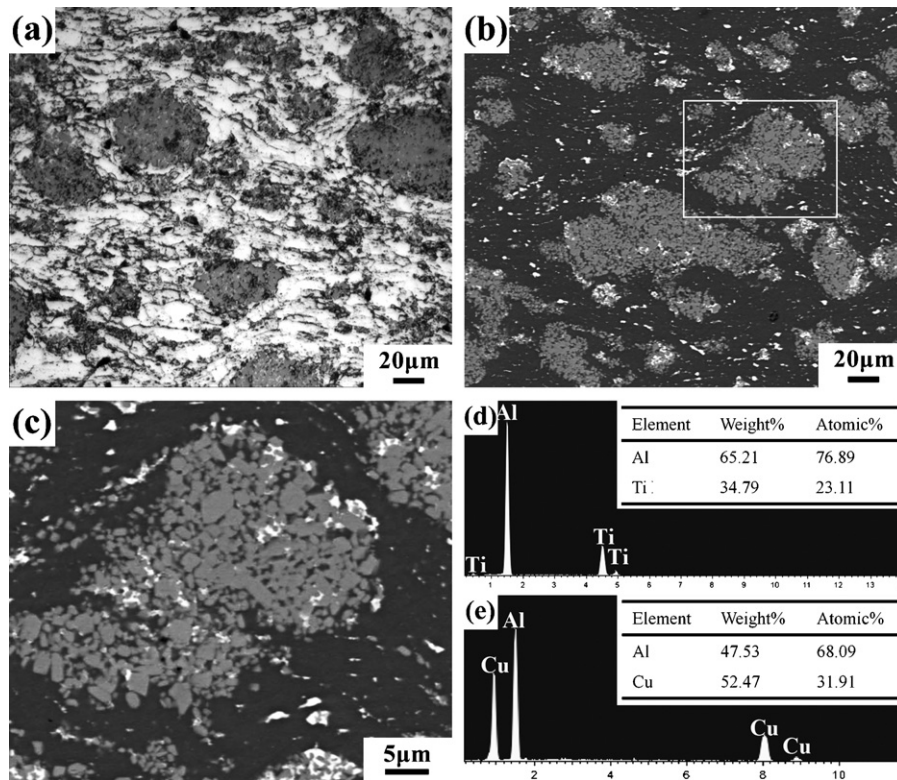
Fig. 3. Microstructure of forged in situ Al$_3$Ti/Al–5.5Cu composite: (a) optical micrograph, (b) SEM micrograph, (c) magnified micrograph of region framed in (b), (d) and (e) EDS spectra of gray and white particles in (c).

water, the matrix grains were refined to approximately 600 nm and a high density of dislocations was often observed in the grains (Fig. 6). The Al$_2$Cu phases were not observed in the FSP-water sample (Fig. 6), which is consistent with the SEM result (Fig. 4(b)).

The DSC curves of the FSP-air and FSP-water samples are shown in Fig. 7. There is a broad exothermic peak at about 307 °C and an endothermic peak at about 524 °C for the FSP-air sample. For the FSP-water sample, the exothermic peak becomes more intensive and the peak temperature decreases to 287 °C. The intensity and location of the endothermic peak in the FSP-water sample did not change compared with that in the FSP-air sample.

Fig. 8 shows the thermal profiles of FSP in air and water respectively. The peak temperature of FSP in air was recorded to be 441 °C, with the temperature above 200 °C for 170 s. For FSP in water, a peak temperature of 352 °C was recorded and the duration above 200 °C was only 7 s.

Fig. 9 shows the TEM images of the aged FSP-water sample. After being aged at 175 °C for 4 h, the grain size did not change visually, whereas the density of dislocations decreased compared with that before aging, and some sub-grains with the characteristics of dislocation recovery were also revealed (as shown by arrows in Fig. 9(a)). Two types of needle-like precipitates with different sizes were found in the Al matrix. Some precipitates had a length of 50–100 nm, while the others had a length of less than 30 nm (Fig. 9(b)).

3.2. Mechanical properties

Tensile properties of in situ Al$_3$Ti/Al–5.5Cu composites under various conditions are summarized in Table 1. The forged sample exhibited a yield strength (YS) of 174 MPa, an ultimate tensile strength (UTS) of 263 MPa and an elongation of 3.5%. Four-pass
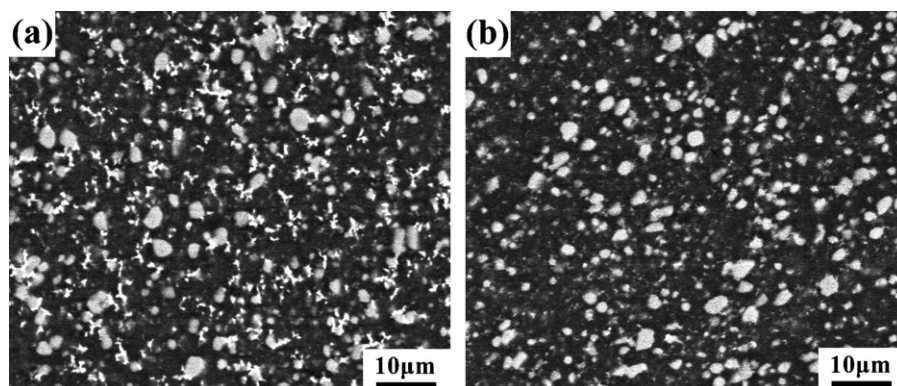
Fig. 4. SEM micrographs of FSP in situ Al$_3$Ti/Al–5.5Cu composite: (a) FSP-air, (b) FSP-water.
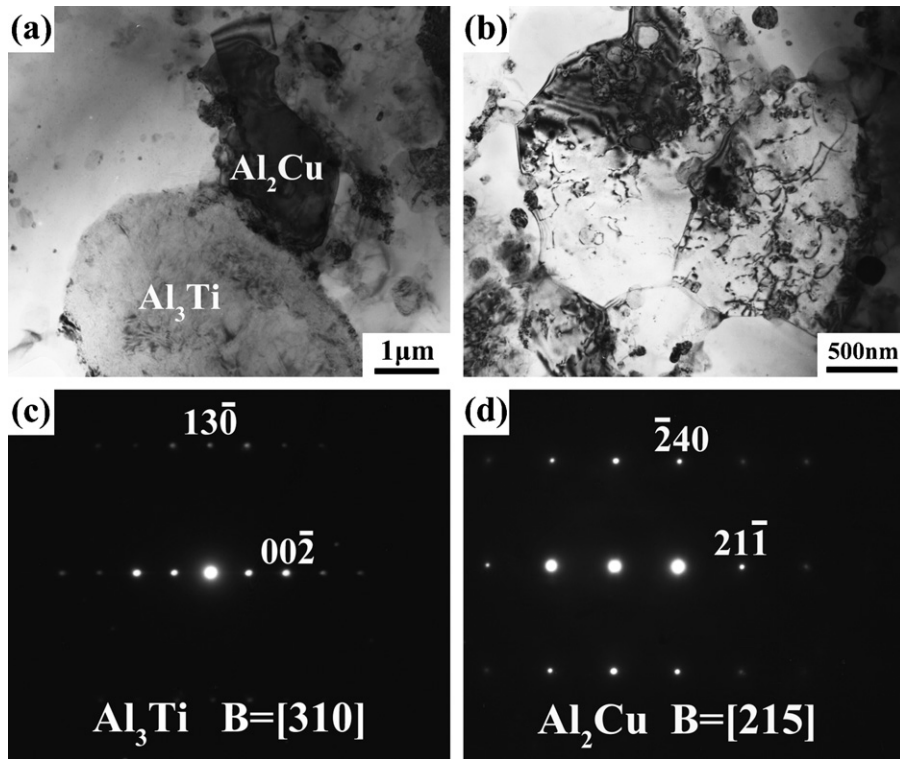
Fig. 5. TEM micrographs of FSP-air sample showing (a) Al₃Ti and Al₂Cu, (b) grains and dislocations, (c) and (d) electron diffraction patterns of Al₃Ti and Al₂Cu.
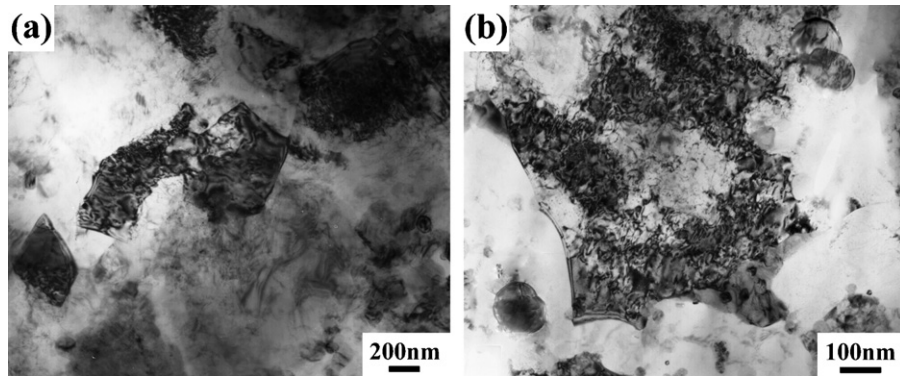
Fig. 6. TEM micrographs of FSP-water sample showing (a) grains and (b) dislocations.

FSP resulted in substantial improvement in the YS (288 MPa), UTS (474 MPa) and elongation (12.0%). Additional 2-pass FSP in water increased the YS (361 MPa) and UTS (577 MPa) further, however, the elongation was reduced to 8.0%. Artificial aging treatment after FSP resulted in a significantly improved YS (417 MPa) and a slightly improved UTS (582 MPa) and elongation (9.0) for the FSP-water sample.

Fig. 10 shows the SEM fractographs of the investigated samples. For the forged sample, the fracture surface was characterized by shallow and coarse dimples with some big pits, in which some par-
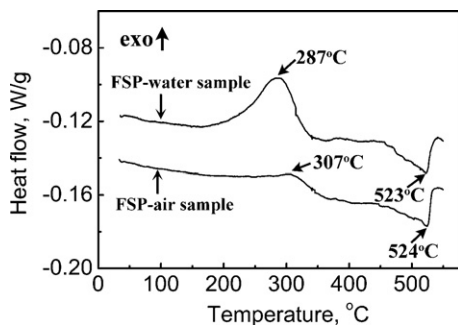
Fig. 7. DSC curves of FSP-air and FSP-water samples.
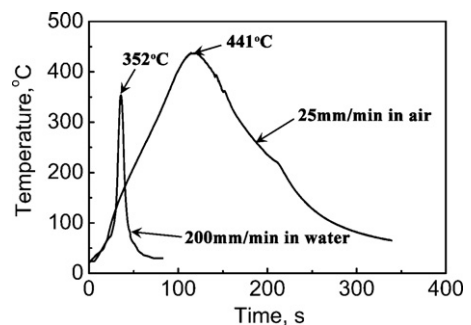
Fig. 8. Thermal profiles of FSP with 25 mm min⁻¹ in air and 200 mm min⁻¹ in water.
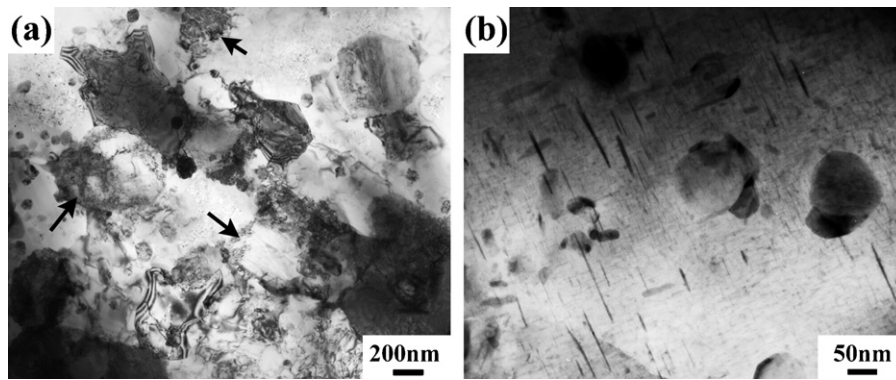
Fig. 9. TEM micrographs of the aged FSP-water sample showing (a) grains and dislocations and (b) precipitates.

Table 1
Tensile properties of forged and FSP samples.

Sample	YS, MPa	UTS, MPa	El., %
Forged	174 ± 2	263 ± 3	3.5 ± 0.5
FSP-air	288 ± 4	474 ± 6	12.0 ± 1.0
FSP-water	361 ± 6	577 ± 7	8.5 ± 1.5
FSP-water + aging	417 ± 5	582 ± 2	9.0 ± 0.5

ticles were revealed (Fig. 10(a)). For the FSP-air sample, a typical ductile dimple-facture morphology was indicated by the equiaxed and fine dimples of 1–3 μm. Furthermore, some holes of 2–3 μm were revealed (white arrows in Fig. 10(b)) on the fracture surface of the FSP-air sample, indicating that some Al$_3$Ti particles de-bonded from the Al matrix during tensile testing. The fracture surface of the FSP-water sample also exhibited some equiaxed and fine dimples of 2–3 μm, but the 2–3 μm holes disappeared (Fig. 10(c)). The

post-FSP aging caused little change in the fracture surface of the FSP-water sample (Fig. 10(d)).

4. Discussion

4.1. Distribution and size of Al$_3$Ti

The XRD and SEM results of the forged sample suggest that all the Ti reacted with Al to form Al$_3$Ti during hot pressing and forging (Figs. 2 and 3). This is different from results reported previously [9,22]. Chianeh et al. [9] fabricated in situ Al$_3$Ti/Al composites from pure Al and Ti powders (63 μm) via powder sintering. Their results indicated that Ti powders could not react with Al completely after the compact was sintered at 600 °C for 5 h. Our previous study [22] also showed that the Al–Ti reaction in an Al–10 at.%Ti compact could not take place completely under the same hot-pressing parameters as reported in this paper. The accelerated forming of Al$_3$Ti in this study could be attributed to the addition of Cu.
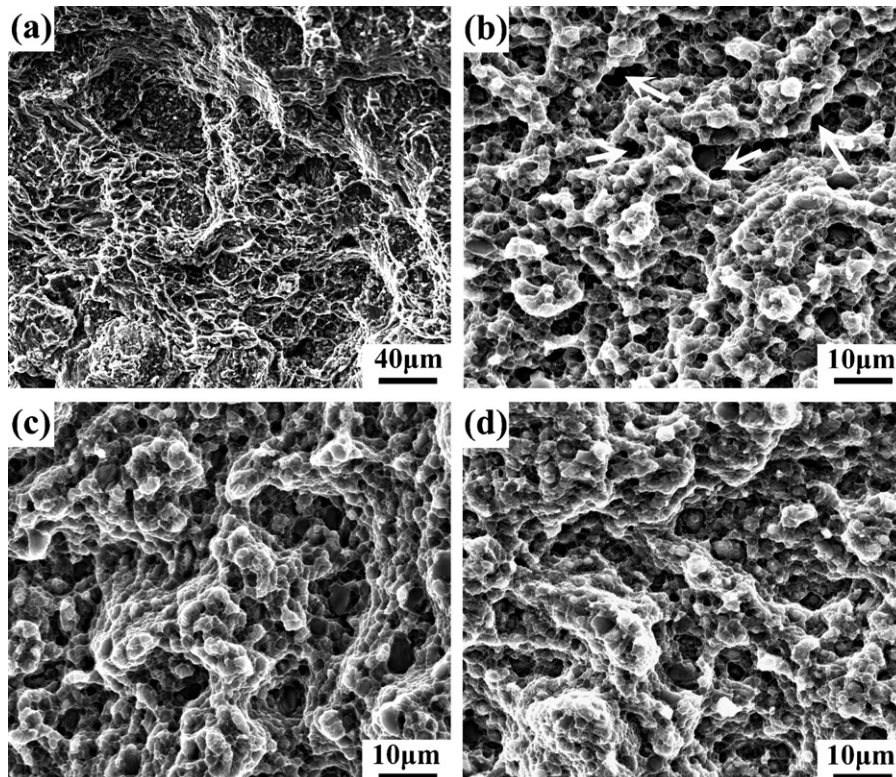
Fig. 10. Fracture surfaces of forged and FSP samples: (a) forged, (b) FSP-air, (c) FSP-water, (d) FSP-water + aging.

During the hot-pressing or sintering of Al–Ti mixed powders, an Al_3Ti layer formed at the Al–Ti interface due to reactive diffusion. Some micro-cracks formed in the Al_3Ti layer due to the volume expansion caused by the transformation from Ti to Al_3Ti [9]. The Al_3Ti layer is the obstacle to the Al–Ti inter-diffusion. In this study, an Al–Cu eutectic liquid phase formed after the compact was heated to 548 °C [23–25] and the liquid phase penetrated into the micro-cracks of the Al_3Ti layers. Thus, the diffusion distance was reduced and the formation of Al_3Ti was accelerated. After the compact was cooled to room temperature, the liquid phase transformed to Al_2Cu in the clearance of Al_3Ti particles (Fig. 3(b) and (c)) [24]. The large brittle Al_3Ti blocks were easily broken into small particles during forging due to the existence of the micro-cracks (Fig. 3(a) and (b)).

During FSP, the material in the SZ experienced intense plastic deformation and thermal exposure. It was estimated that 1-pass FSP could produce an effective strain of >40 [26]. Intense deformation broke up the Al_3Ti blocks and resulted in a uniform distribution of the Al_3Ti particles. However, although a small quantity of nano-sized Al_3Ti particles formed due to the intense breaking effect of the threaded pins, most of the Al_3Ti particles were still in the range of 1–3 μm (Fig. 4), which is similar to that in the forged sample (Fig. 3(b) and (c)).

According to previous studies [13,17], the refining of second-phase particles during FSP depends on not only the tool geometry and processing parameters, but also the stiffness, ductility, strength of the matrix and the initial size and aspect ratio of the particles. For example, FSP with a tool rotation rate of 300–900 rpm broke up the acicular Si particles in sand-cast A356 alloys, resulting in the uniform distribution of fine Si particles with an average size of 2–3 μm and an average aspect ratio of ~2.0. However, increasing the tool rotation rate from 900 rpm to 1100 rpm did not result in any further refinement of the Si particles [13]. In the present study, Fig. 3(c) revealed that the Al_3Ti blocks consisted of numerous Al_3Ti particles 1–4 μm in diameter with a small aspect ratio. These fine particles could flow with the matrix during FSP under the relatively high rotation rate of 1000 rpm. In this case, although the distribution of the Al_3Ti was significantly improved by 4-pass FSP, the refining of the Al_3Ti particles was limited. Additional 2-pass FSP in water caused little influence on the size of the Al_3Ti particles (Fig. 4).

4.2. Grain morphology and dislocation structure

As shown in Fig. 3(a), the matrix of the forged sample was composed of some elongated and equiaxed grains with a size of 10–20 μm. The elongated grains were caused by the plastic flow of the matrix during forging and the equiaxed grains indicated that recovery and partial recrystallization occurred during forging and subsequent cooling [27]. These original grain structures were completely eliminated and replaced by the fine equiaxed grains with a low density of dislocation after 4-pass FSP in air (Fig. 5(b)).

The fine grain structure in the FSP-air sample resulted from dynamic recrystallization during FSP, created by local thermal exposure and severe plastic strain. It has been reported that newly recrystallized grains 25–100 nm in diameter formed around the pin tool during FSP [28,29]. During subsequent processing, the initial microstructures evolved due to the thermo-mechanical deformation behind the pin tool. The process included grain growth, introduction of additional dislocations and recovery in the grains [20]. For FSP in air in the present study, a relatively high tool rotation rate and low traverse speed were adopted. The duration of the temperature above 200 °C (recovery temperature of some Al alloys) during FSP was about 170 s (Fig. 8). Growth of the grains would occur but dislocation generated by severe plastic strain would be annihilated due to dynamic recovery in the long duration of thermal exposure. Nevertheless, the grain size in the FSP-air sample was still smaller than that reported in most of FSW/FSP Al alloys

[30]. This can be attributed to the inhibiting and pining effects of the Al_3Ti particles on the growth of the grains.

For the FSP-water sample, the traverse speed of FSP increased to 200 mm min^{-1} and additional rapid cooling with flowing water was used in order to increase the cooling rate after FSP. The thermal history indicated that the duration of the temperature above 200 °C during FSP in water was only 7 s (Fig. 8). In this case, the growth of the recrystallized grains was effectively inhibited and more dislocations were retained (Fig. 6). However, the density of dislocations in the FSP-water sample was somewhat higher than that reported in FSP Al–Mg–Sc [31] and 7075Al [20] processed in water with similar parameters. This can be attributed to several factors. Firstly, some "geometrically necessary" dislocations would be generated during the deformation due to the difference of elastic moduli between the Al_3Ti and Al matrix [32]. Secondly, some thermal mismatch dislocations would be generated due to the difference of CTE between the Al_3Ti and Al matrix during rapid cooling [2].

The high density of dislocations in the FSP-water sample were recovered during the artificial aging at 175 °C for 4 h and formed some sub-structures in the Al matrix (Fig. 9(a)). Furthermore, because the aging time was short the grains did not grow (Fig. 9(a)). The results of Cheng et al. [33] indicate that the growth of the nano-sized recrystallized grains of 2024Al occurred after aging at 160 °C for 13 h.

4.3. Dissolution and re-precipitation of Al_2Cu

Figs. 2 and 3 show that some Al_2Cu particles with a size of 1–2 μm were formed in the forged sample. Apart from being located in the clearance of Al_3Ti clusters (Section 4.1), the Al_2Cu particles were usually located at the Al/Al_3Ti interface or formed a (semi) network in the matrix. As discussed in Section 4.1, when the cold compact was heated above the eutectic temperature of Al–Al_2Cu, some transient liquid phase would form. Besides penetrating into the micro-cracks of the Al_3Ti layers, the transient liquid phase would wet the outside of the oxide-covered Al particles and penetrate into the particle contacts [25]. During the subsequent holding at 600 °C, Cu would be drawn from the liquid phase into the solid solution of aluminum [34]. Because the Cu addition was 5.5 wt% in the present study, which is higher than the equilibrium solubility of Cu in Al at 600 °C according to the Al–Cu phase diagram, so some liquid would be retained in the particles contacts, such as Al–Al particles boundaries and Al/Al_3Ti interface. The existence of liquid in the particles contacts would facilitate the densification of the compact during hot pressing. After the compact was cooled to room temperature, the liquid phase would transform to Al_2Cu [24,34] at the Al/Al_3Ti interfaces or at the initial Al particles boundaries, forming a (semi) network. Furthermore, some Al_2Cu would precipitate preferentially at these locations from the matrix where the free energy was higher than the other locations during the cooling. In the present study, forging did not change the distribution of the Al_2Cu particles substantially due to the lower temperature and deformation ratio of the forging.

After 4-pass FSP in air, some Al_2Cu particles of similar size remained (Figs. 4(a) and 5(a)). Previous studies suggested that FSP functions like a solution treatment, though the duration of thermal exposure during FSP was shorter compared with that of conventional solution treatment [13,18,19]. The accelerated dissolution is usually attributed to the significantly accelerated diffusion rate and shortened diffusion distance caused by severe plastic deformation of FSP [35].

The peak temperatures during FSW/FSP recorded by embedded thermocouples in the regions adjacent to the rotating pin were generally reported to be in the range of 400–500 °C [30]. Fig. 8 indicates that the peak temperature in the bottom of the SZ during FSP in air was 441 °C. This is in agreement with those reported in

FSP/W aluminum alloys [30]. It is important to note that the actual peak temperature of the SZ during FSP should be higher than that recorded by the thermocouple. Thus, most of the Al_2Cu particles in the forged sample should dissolve into the Al matrix during 4-pass FSP in air.

However, some Al_2Cu particles were still found in the FSP-air sample (Figs. 4(a) and 5(a)). This can be explained as follows. Firstly, the traverse speed for the FSP-air sample was relatively low, causing a long duration of thermal exposure. The duration of the temperature above 200 °C during FSP was as long as 170 s as shown in Fig. 8. The Al_2Cu would re-precipitate and coarsen over such a long duration. Secondly, as discussed above, the density of dislocations in the composites during FSP was higher than that in the aluminum alloys. The increased density of dislocations would accelerate the forming and coarsening of Al_2Cu. The weak exothermic peak corresponding to the precipitation of Al_2Cu in the DSC curve further proved that most of Al_2Cu phase had precipitated from the matrix in the FSP-air sample (Fig. 7). Thirdly, some coarse Al_2Cu particles might be not fully dissolved during FSP thermal exposure and remained in the matrix.

Although the peak temperature in the bottom of the SZ during FSP in water was only 352 °C (Fig. 8), Figs. 4(b) and 6 show that additional 2-pass FSP in water still resulted in the dissolution of the Al_2Cu. This may also be attributed to the accelerated diffusion rate and shortened diffusion distance caused by severe plastic deformation of FSP [35]. However, because the traverse speed of FSP was increased to 200 mm min^{-1} and additional rapid cooling with flowing water was used during FSP, the duration of the temperature above 200 °C during FSP was reduced to 7 s (Fig. 8). In this case, the precipitation of Al_2Cu was prohibited [36,37]. During the heating of the DSC experiment, the precipitation of the Al_2Cu phase resulted in an intense exothermic peak at 287 °C for the FSP-water sample (Fig. 7).

Aging at 175 °C for 4 h for the FSP-water sample resulted in the precipitation of some metastable phases of Al_2Cu from the supersaturated solid solution (Fig. 9(b)). The precipitation sequence of Al_2Cu has been well documented [36,37]. The needle-like precipitates with a length of 50–100 nm would be θ', and those with a length less than 30 nm would be θ''. A large number of θ'' coexisting with a small quantity of θ' indicate that the FSP-water sample has effectively been peak aged [37]. Although two types of precipitates were revealed in Fig. 9(b), only one exothermic peak in the DSC curve of the FSP-water sample was observed (Fig. 7). This may be attributed to the acceleration of aging caused by reinforcement addition or high density of dislocations in the matrix. The precipitation kinetics of the FSP samples especially the FSP-water sample needs a further research.

4.4. Tensile properties

As presented in Fig. 3(a), the microstructure of the forged sample is characterized by coarse Al_3Ti clusters between 50 and 100 μm. These Al_3Ti clusters consisted of numerous Al_3Ti particles between 1 and 4 μm (Fig. 3(c)). Micro-cracks would form preferentially in the coarse Al_3Ti clusters during tensile testing, resulting in a reduction in the tensile strength and ductility and leaving some big pits with some Al_3Ti particles on the fracture surface (Fig. 10a).

Four-pass FSP in air resulted in a significant improvement in both strength and ductility. This is attributed to the refinement and redistribution of Al_3Ti by FSP (Fig. 4(a)). The refinement and redistribution of the coarse Al_3Ti clusters significantly reduces the possibility of the Al_3Ti cluster cracking under low stress. Consequently, the possibility of void initiation is minimized, thereby simultaneously increasing the strength and ductility of the composite. Meanwhile, the uniform distribution of the Al_3Ti particles reduced the mean inter-particle distance and then resulted

in the equiaxed and fine dimples on the fracture surface in the FSP-air sample (Fig. 10(b)). However, some Al_2Cu particles formed due to the relatively long thermal exposure of FSP in air (Figs. 4(a) and 5(a)). Firstly, the formation of Al_2Cu reduced the concentration of Cu in the Al matrix. This in turn reduced the solution and aging strengthening effects produced by Cu addition. Secondly, the Al_2Cu particles generally formed at the Al/Al_3Ti interface (Fig. 5(a)), resulting in a reduction in interfacial bonding strength. During the tensile test, some Al_3Ti de-bonded from the matrix due to the low interfacial strength, leaving some holes on the fracture surface as shown in Fig. 10(b).

Additional 2-pass FSP in water caused little influence on the distribution and size of the Al_3Ti particles, so the size and morphology of the dimples on the fracture surface almost did not change. However, additional 2-pass FSP in water dissolved most of the Al_2Cu into the Al matrix (Fig. 4(b)). The dissolution of Al_2Cu increased the strength of the matrix due to the solution strengthening effect, reducing the probability of de-bonding of the Al_3Ti/Al interface during tensile testing. Furthermore, the matrix grains were refined significantly and the density of dislocations increased in the FSP-water sample (Fig. 6). Thus, the YS and UTS increased and the ductility decreased in the FSP-water sample.

Aging at 175 °C for 4 h for the FSP-water sample resulted in the precipitation of fine θ'' and θ' phases (Fig. 9(b)), thereby increasing the YS and the UTS of the sample. However, the ductility of the aged sample did not decrease in comparison with that non-aged sample. This may be associated with the decrease in dislocation density after aging (Fig. 9(a)). The low dislocation density after aging would provide more room for dislocation accumulation during tensile testing, leading to an improved ductility. A similar result was reported in cryo-rolled 2024Al [33,38] and equal channel angular pressed 6061Al [39]. Generally, for the PRAMCs, the improvement of the matrix strength would cause more particles to crack during tensile test [40], which can be revealed on the fracture surface. In the present study, although the matrix strength of the FSP-water sample was improved after aging, no cracked Al_3Ti particles were observed on the fracture surfaces, indicating that the stress on the Al_3Ti particles was still not beyond its fracture strength during tensile test. So for the FSP-water sample, the post-FSP aging caused little change on the fracture surface.

5. Conclusions

(1) Cu addition accelerated the formation of Al_3Ti during hot pressing at 600 °C, with all the Ti reacting with the Al to form Al_3Ti during the hot pressing and subsequent forging. This formed an in situ Al_3Ti/Al–5.5Cu composite.

(2) The forged composite was characterized by the coarse matrix grains and coarse Al_3Ti clusters with a size of 50–100 μm, with the Al_2Cu particles distributed in the matrix or the clearance of the Al_3Ti clusters. These microstructural characteristics led to lower strength and ductility of the forged composite.

(3) Four-pass FSP in air resulted in the refinement and redistribution of the Al_3Ti clusters and the generation of fine matrix grains. Meanwhile, the Al_2Cu dissolved and re-precipitated due to a relatively long duration of thermal exposure. These resulted in a simultaneous increase in the strength and ductility.

(4) Additional 2-pass FSP in water produced little influence on the distribution and size of the Al_3Ti particles, but most of the Al_2Cu was dissolved into the matrix with the solutes retained in solution due to the short duration of thermal exposure. Additionally, the ultrafine matrix grains with a high density of dislocations were obtained. These microstructure changes resulted in a significant increase in strengths and a decrease in ductility.

(5) Post-FSP aging resulted in the precipitation of metastable phases of Al_2Cu and an increase in the YS and the UTS of the FSP-water sample. The ductility of the aged FSP-water sample did not decrease due to the reduction in dislocation density after aging compared with that of the FSP-water sample.

Acknowledgments

References

[1] D.B. Miracle, Compos. Sci. Technol. 65 (2005) 2526.
[2] D.J. Lloyd, Int. Mater. Rev. 39 (1994) 1.
[3] J.M. Torralba, C.E. da Costa, F. Velasco, J. Mater. Process. Technol. 133 (2003) 203.
[4] A.L. Geiger, J.A. Walker, JOM 43 (1991) 8.
[5] M.Z. Tan, Q.B. Xin, Z.G. Li, B.Y. Zong, J. Mater. Sci. 36 (2001) 2045.
[6] B. Torres, M. Lieblich, J. Ibanez, A.G. Escorial, Scripta Mater. 47 (2002) 45.
[7] T.Z. Li, E.A. Olevsky, M.A. Meyers, Mater. Sci. Eng. A 473 (2008) 49.
[8] D. Roy, S. Ghosh, A. Basumallick, B. Basu, J. Alloys Compd. 436 (2007) 107.
[9] V.A. Chianeh, H.R.M. Hosseini, M. Nofar, J. Alloys Compd. 473 (2009) 127.
[10] K. Das, L.K Narnaware, Mater. Charact. 60 (2009) 808.
[11] R.A. Varin, Metall. Mater. Trans. A 33 (2002) 193.
[12] R.S. Mishra, M.W. Mahoney, S.X. Mcfadden, N.A. Mara, A.K. Mukherjee, Scripta Mater. 42 (2000) 163.
[13] Z.Y. Ma, S.R. Sharma, R.S. Mishra, Metall. Mater. Trans. A 37 (2006) 3323.
[14] D. Zhang, M. Suzuki, K. Maruyama, Scripta Mater. 52 (2005) 899.
[15] C.J. Hsu, C.Y. Chang, P.K. Kao, N.J. Ho, C.P. Chang, Acta Mater. 54 (2006) 5241.
[16] C.J. Hsu, P.W. Kao, N.J. Ho, Mater. Lett. 61 (2007) 1315.
[17] X.G. Chen, M.D. Silva, P. Gougeon, L.S. Georges, Mater. Sci. Eng. A 518 (2009) 174.
[18] Y.S. Sato, H. Kokawa, M. Enomoto, S. Jogan, Metall. Mater. Trans. A 30 (1999) 2429.
[19] B.L. Xiao, Q. Yang, J. Yang, W.G. Wang, G.M. Xie, Z.Y. Ma, J. Alloys Compd. 509 (2011) 2879.
[20] J.Q. Su, T.W. Nelson, C.J. Sterling, Scripta Mater. 52 (2005) 135.
[21] J.Q. Su, T.W. Nelson, T.R. McNelley, R.S. Mishra, Mater. Sci. Eng. A 528 (2011) 5458.
[22] Q. Zhang, B.L. Xiao, D. Wang, Z.Y. Ma, Mater. Chem. Phys. 130 (2011) 1109.
[23] B. Ogel, R. Gurbuz, Mater. Sci. Eng. A 301 (2001) 213.
[24] J. Zhou, J. Duszczyk, J. Mater. Sci. 34 (1999) 545.
[25] W. Kehl, H.F. Fischmeister, Powder Metall. 23 (1980) 113.
[26] P. Heurtier, C. Desrayaud, F. Montheillet, Mater. Sci. Forum 1537 (2002) 396–402.
[27] M. Vedani, F.D. Errico, E. Gariboldi, Compos. Sci. Technol. 66 (2006) 343.
[28] C.G. Rhodes, M.W. Mahoney, W.H. Bingel, M. Calabrese, Scripta Mater. 48 (2003) 1451.
[29] R.W. Fonda, J.F. Bingert, K.J. Colligan, Scripta Mater. 51 (2004) 243.
[30] R.S. Mishra, Z.Y. Ma, Mater. Sci. Eng. Rep. 50 (2005) 1.
[31] F.C. Liu, Z.Y. Ma, L.Q. Chen, Scripta Mater. 60 (2009) 968.
[32] T.S. Srivatsan, M.A. Hajri, C. Smith, M. Petraroli, Mater. Sci. Eng. A 346 (2003) 91.
[33] S. Cheng, Y.H. Zhao, Y.T. Zhu, E. Ma, Acta Mater. 55 (2007) 5822.
[34] Q. Zhang, B.L. Xiao, Z.Y. Liu, Z.Y. Ma, J. Mater. Sci. 46 (2011) 6783.
[35] Z.Y. Ma, A.L. Pilchak, M.C. Juhas, J.C. Williams, Scripta Mater. 58 (2008) 361.
[36] H.K. Hardy, J. Inst. Met. 83 (1954) 17.
[37] L.F. Mondolfo, Aluminum Structure and Properties, Butterworth & Co. Ltd, London, 1979.
[38] Y.J. Huang, Z.G. Chen, Z.Q. Zheng, Scripta Mater. 64 (2011) 382.
[39] W.J. Kim, J.K. Kim, T.Y. Park, S.I. Hong, D.I. Kim, Y.S. Kim, J.D. Lee, Metall. Mater. Trans. A 33 (2002) 3155.
[40] D.J. Lloyd, Acta. Metall. Mater. 39 (1991) 59.